

# Robot Design Optimization with Rotational and Prismatic Joints using Black-Box Multi-Objective Optimization

Kento Kawaharazuka<sup>1</sup>, Kei Okada<sup>1</sup>, and Masayuki Inaba<sup>1</sup>

**Abstract**—Robots generally have a structure that combines rotational joints and links in a serial fashion. On the other hand, various joint mechanisms are being utilized in practice, such as prismatic joints, closed links, and wire-driven systems. Previous research have focused on individual mechanisms, proposing methods to design robots capable of achieving given tasks by optimizing the length of links and the arrangement of the joints. In this study, we propose a method for the design optimization of robots that combine different types of joints, specifically rotational and prismatic joints. The objective is to automatically generate a robot that minimizes the number of joints and link lengths while accomplishing a desired task, by utilizing a black-box multi-objective optimization approach. This enables the simultaneous observation of a diverse range of body designs through the obtained Pareto solutions. Our findings confirm the emergence of practical and known combinations of rotational and prismatic joints, as well as the discovery of novel joint combinations.

## I. INTRODUCTION

Robots typically feature a structure that combines rotational joints and links in a serial manner [1], [2]. On the other hand, in practice, there exist various joint mechanisms such as prismatic joints [3], [4], closed links [5], and wire-driven systems [6], [7]. Historically, these designs have been manually crafted by humans, but there are numerous initiatives aimed at automating these processes.

[8] optimized the number and types of one-axis rotational joint modules, as well as their relative positions, for industrial robots using a genetic algorithm to achieve desired operational points. [9] optimized the motors and gear ratios of a general serial-link 6-DOF manipulator based on weight minimization and manipulability maximization, though it does not involve modular robots. [10] performed multi-objective optimization for a modular robot composed of one-axis rotational joints, focusing on minimizing positional error and force for daily life support. In the realm of closed-link structures, [11] optimized the link lengths and configurations. For wire-driven systems, [12] optimized the wire attachment positions for a parallel wire-driven robot using evolutionary computation. [13] extended [12] to include wire attachment links under selectable conditions, enabling more complex optimization.

Despite various research efforts in design optimization, the focus has predominantly been on optimizing individual mechanical structures. Notably, there have been several recent studies specifically addressing design optimization of

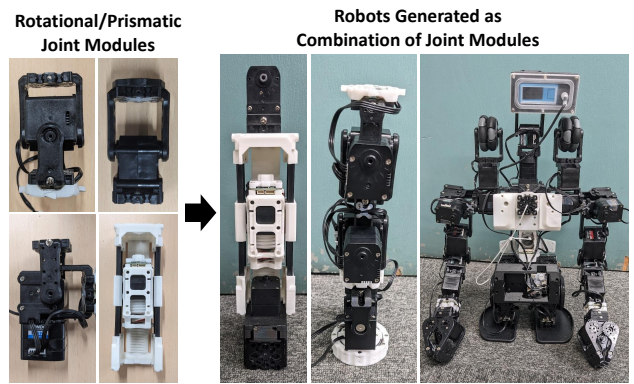


Fig. 1. Examples of rotational and prismatic joint modules, as well as robots generated through their combinations.

bodies incorporating one-axis rotational joints and rotational wheels. [14], [15] optimized the joint arrangement and discrete values of link lengths for a modular robot capable of traversing uneven terrain. Similarly, [16] conducted design optimization for a modular robot adept at navigating rough terrain, utilizing Generative Adversarial Network (GAN) for diverse body generation.

On the other hand, despite the existence of numerous combinations of various joint mechanisms, a considerable portion of them remain unexplored. More specifically, examples that combine prismatic joints, closed-link structures, and wire-driven systems are not apparent, leaving untapped potential for numerous valuable solutions. Fig. 1 illustrates such examples, showcasing the possibility of constructing diverse robot bodies through various combinations of joint structures. These constructions should not be limited to human-designed solutions but should be autonomously discovered. Therefore, in this study, we conduct design optimization for robots by combining multiple joint structures, particularly incorporating both rotational and prismatic joints. Each joint structure is modularized and described as an individual file, forming the robot model through their combinations. The objective is to minimize the number of joints and link lengths while achieving the given task, employing a black-box multi-objective optimization for automatic design optimization. This research stands out from previous studies by not only focusing on robot performance but also emphasizing design aspects such as minimizing the number of joints and link lengths. Additionally, by intentionally avoiding a single objective function and employing multi-objective optimization, we can obtain a multitude of solutions with varying degrees of freedom as Pareto solutions, allowing us to grasp the

<sup>1</sup> The authors are with the Department of Mechano-Informatics, Graduate School of Information Science and Technology, The University of Tokyo, 7-3-1 Hongo, Bunkyo-ku, Tokyo, 113-8656, Japan. [kawaharazuka, k-okada, inaba]@jsk.t.u-tokyo.ac.jp

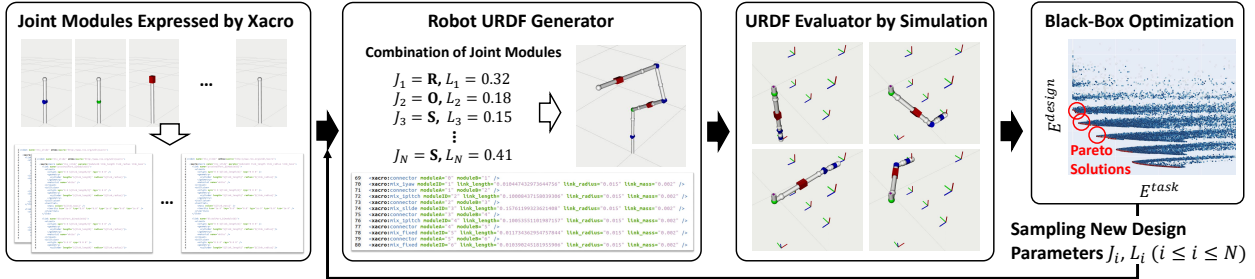


Fig. 2. The overview of the proposed system. Joint modules are expressed using Xacro, and a robot URDF is generated by combining these modules. The generated URDF is then evaluated through simulation, and the subsequent designs are iteratively generated by black-box optimization.

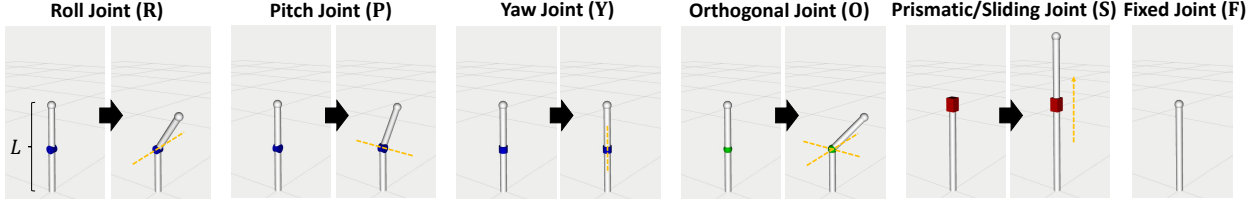


Fig. 3. The joint modules used in this study. The roll joint (**R**), the pitch joint (**P**), the yaw joint (**Y**), the two-axis orthogonal joint (**O**), the prismatic/sliding joint (**S**), and the fixed joint (**F**) are predefined. The design parameters encompass the type of the joint module and the length of the link  $L$ .

characteristics of each design. From the obtained Pareto solutions, we confirmed the emergence of practical and known combinations of rotational and prismatic joints, as well as the discovery of novel joint combinations.

The structure of this study is outlined as follows. In Section II, we elaborate on design parameters, the definition of objective functions, and multi-objective optimization. In Section III, we apply the proposed method to optimize robot design for achieving three specific tasks. Finally, in Section IV, we present conclusions and future prospects.

## II. ROBOT DESIGN OPTIMIZATION WITH ROTATIONAL AND PRISMATIC JOINTS USING BLACK-BOX MULTI-OBJECTIVE OPTIMIZATION

The overall system is illustrated in Fig. 2. Each joint module is described using Xacro (XML Macros), and these modules are combined to generate the URDF (Unified Robot Description Format) of the robot. This URDF is then evaluated through simulation, and new design parameters are iteratively generated using black-box optimization. In this section, we first discuss the structure of each joint module, how they interconnect to form a unified robot, and describe the set of body parameters. Next, we define objective functions to evaluate these parameters and describe black-box multi-objective optimization based on these evaluations.

### A. Design Parameters

We first describe the prerequisites for the body design. We denote the position and orientation of the robot's root link as  $\mathbf{p}^{root}$  and  $\mathbf{R}^{root}$ , respectively. Similarly, the position and orientation of the effector are represented as  $\mathbf{p}^{ee}$  and  $\mathbf{R}^{ee}$ . In the initial pose, where all joint angles and positions are set to 0, we configure the links in a straight line. This configuration is similar to that of industrial robots and humanoids; for example, the arms and legs of a humanoid would be straightened in the initial pose. While alternative

configurations are possible, we adopt this general assumption here.

Next, we elaborate on each module constituting the robot. This study focuses on rotational joints and prismatic joints, with particular emphasis on various configurations, especially in the case of rotational joints. The one-axis rotational joints for roll **R**, pitch **P**, and yaw **Y**, as well as the commonly used orthogonal two-axis joint **O** for roll and pitch, are considered. Adding a prismatic joint **S**, we illustrate the five joints in Fig. 3. Each module has a parameter  $L$  representing its length, indicating the total length of the module in the initial pose. Rotational joints are positioned between two links of length  $L/2$ . Prismatic joints start with an initial state featuring a link of length  $L$  and can extend up to  $2L$ . Additionally, each joint module has a range of motion denoted as  $\theta^{\{min,max\}}$ . In this study, considering general range of motion limits, we set  $\theta^{\{min,max\}} = \{-3/4\pi, 3/4\pi\}$  for roll and pitch (including orthogonal two-axis joints),  $\theta^{\{min,max\}} = \{-2\pi, 2\pi\}$  for yaw, and  $\theta^{\{min,max\}} = \{0, L\}$  for prismatic joints. However, for optimization, the number of parameters to optimize must be predetermined. Therefore, to avoid initially fixing the number of joints in the robot to be designed, we introduce an additional joint, a fixed joint **F**. This joint is also represented as a link of length  $L$ , with no articulated joint, and  $\theta^{\{min,max\}} = \{0, 0\}$ . These six modules are described in Xacro format.

Finally, we combine these modules to construct a robot model. By connecting the distal link of the  $i$ -th module with the proximal link of the  $(i+1)$ -th module, the links are joined. Therefore, with the number of modules included in a single robot denoted as  $N^{jnt}$ , the design parameters consist of six discrete parameters  $J_i$  ( $1 \leq i \leq N^{jnt}$ ) representing the choices of the six joint types:  $\{\mathbf{R}, \mathbf{P}, \mathbf{Y}, \mathbf{O}, \mathbf{S}, \mathbf{F}\}$ , and continuous parameters  $L_i$  representing the link lengths. Here, careful consideration is needed for the

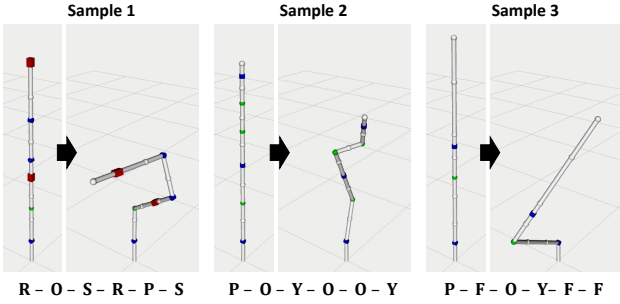


Fig. 4. The random robot models generated through the combination of predefined joint modules.

range  $[L_i^{\min}, L_i^{\max}]$  of  $L_i$ . When  $L_i$  is very small, it becomes challenging to construct actual modules especially for roll, pitch, and prismatic joints. Therefore, in this study, the range of  $L_i$  for **R**, **P**, **O**, **S** is set as  $[0.1, 0.5]$ , while for **Y** and **F**, it is set as  $[0.01, 0.5]$ . During actual optimization, continuous parameters  $C_i$  with a range of  $[0.0, 1.0]$  are optimized, and we set  $L_i = (L_i^{\max} - L_i^{\min})C_i + L_i^{\min}$ .

The robots constructed with random parameters are shown in Fig. 4. It can be observed that diverse body structures are represented by the parameters of the six module types and their corresponding lengths.

### B. Objective Functions and Black-Box Multi-Objective Optimization

First, we discuss the objective functions to be optimized. Since it is a multi-objective optimization, multiple objective functions can be specified. In this study, two objective functions are used from the perspective of visibility.

The first one is the task accomplishment of the robot, denoted by the objective function  $E_i^{\text{task}}$ . It is defined as the minimization of whether the specified  $N^{\text{ref}}$  positions and orientations  $(p_i^{\text{ref}}, R_i^{\text{ref}})$  ( $1 \leq i \leq N^{\text{ref}}$ ) are achieved by the robot's end effector, as follows,

$$q_i = \text{IK}(p_i^{\text{ref}}, R_i^{\text{ref}}) \quad (1)$$

$$E_i^{\text{task}} = \|e(q_i)\|_2 \quad (2)$$

$$E^{\text{task}} = \sum_{i=1}^{N^{\text{ref}}} E_i^{\text{task}} \quad (3)$$

where  $q_i$  represents the joint angles obtained by solving the inverse kinematics **IK**,  $e(q_i)$  is the error vector (the upper 3 components represent the positional error and the lower 3 components represent the rotational error), and  $\|\cdot\|_2$  denotes the L2 norm. In other words, the sum of errors in inverse kinematics constitutes  $E^{\text{task}}$ . While more complex tasks or dynamic movements, such as walking, can be considered, this study focuses on a configuration that specifically examines the simplest kinematics.

The second objective function is the minimization of the number of joints and link lengths, defined as  $E^{\text{design}}$ . It is

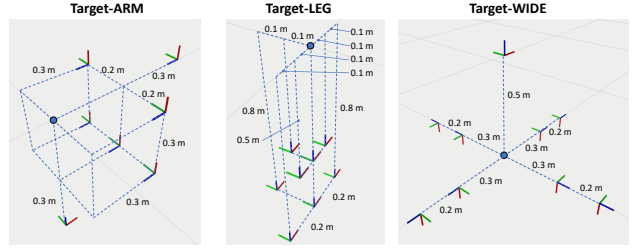


Fig. 5. Three types of target positions and orientations: Target-ARM, Target-LEG, and Target-WIDE.

defined as follows,

$$E_{\text{joint}}^{\text{design}} = N_R^{\text{jnt}} + N_P^{\text{jnt}} + N_Y^{\text{jnt}} + 2N_O^{\text{jnt}} + N_S^{\text{jnt}} \quad (4)$$

$$E_{\text{length}}^{\text{design}} = \sum_{i=1}^{N^{\text{jnt}}} L_i \quad (5)$$

$$E^{\text{design}} = E_{\text{joint}}^{\text{design}} + E_{\text{length}}^{\text{design}} \quad (6)$$

where  $N_{\{R, P, Y, O, S\}}^{\text{jnt}}$  represents the number of occurrences of **R**, **P**, **Y**, **O**, **S**.

Next, we delve into multi-objective optimization. In typical optimization scenarios, weights are applied to multiple objective functions, and they are transformed into a single objective function for optimization. However, this study aims to discover new body morphologies by generating diverse solutions with inherent trade-offs. Therefore, intentionally avoiding narrowing down the solutions to a single one, multi-objective optimization is performed based on the two objective functions, presenting a diverse set of Pareto solutions. For this purpose, we employ the NSGA-II algorithm [17] from the Optuna library [18] for black-box optimization. The number of trials varies slightly for each task, being around 70,000, and the execution time is approximately 5 hours.

## III. SIMULATION EXPERIMENTS

### A. Experimental Setup

In this study, three experiments were conducted while varying the configuration of  $(p_i^{\text{ref}}, R_i^{\text{ref}})$ , as shown in Fig. 5. The first experiment, Target-ARM, comprises seven target positions and orientations feasible for human arms. The second experiment, Target-LEG, comprises eight target positions and orientations feasible for human legs. The third experiment, Target-WIDE, comprises nine target positions and orientations, particularly covering a wider range suitable for industrial robots. Note that  $N^{\text{jnt}}$  was set to 6 for all experiments.

### B. Results for Target-ARM

For Target-ARM, the obtained Pareto solutions are shown in Fig. 6, and the sampling results are shown in Fig. 7.

First, we explain how to interpret the results. In Fig. 7, each point represents a single solution in the sampling process. Among these, the red points denote Pareto solutions, indicating superior trade-offs between the horizontal axis  $E^{\text{task}}$  and the vertical axis  $E^{\text{design}}$ . In this study, multiple

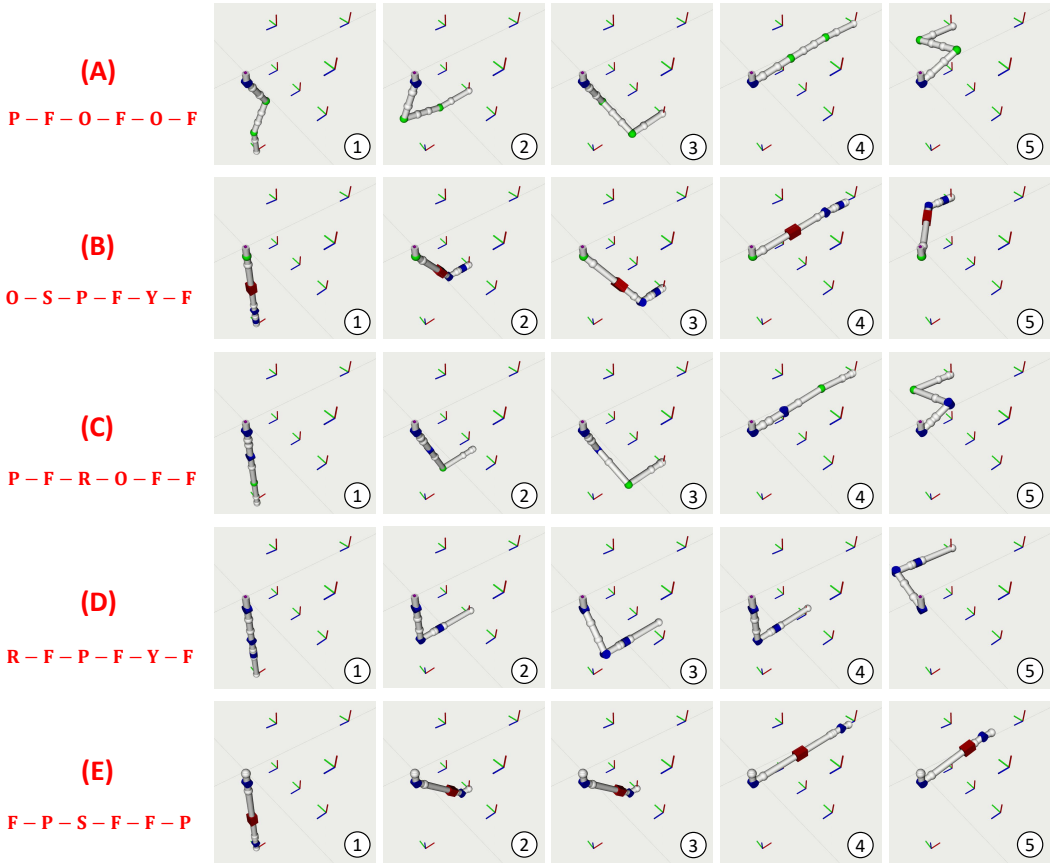


Fig. 6. Several representative Pareto solutions for Target-ARM. Each snapshot shows the result of inverse kinematics for the target position and orientation.

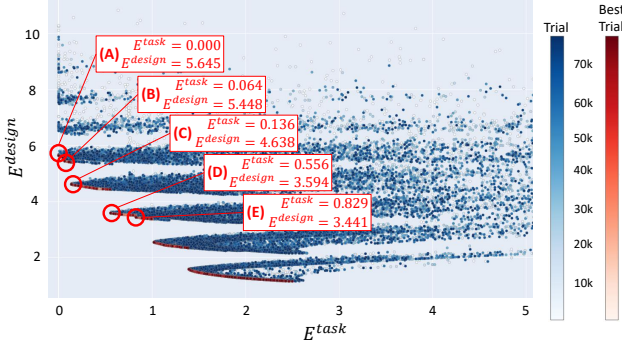


Fig. 7. Sampling results for Target-ARM. Each point represents a solution, with the Pareto solutions highlighted in red. Solutions (A) to (E) are the representative solutions in Fig. 6.

solutions with different configurations among the Pareto solutions were extracted and presented in Fig. 6. ①–⑤ depict the inverse kinematics solutions for each target pose in Target-ARM shown in Fig. 5. In the case of symmetrical configurations, some solutions are omitted for clarity. Additionally, regarding the values of  $E^{design}$ , it should be noted that in this study, as the robot's total length  $E_{length}$  never exceeded 1, the integer part of  $E^{design}$  represents the degrees of freedom  $E_{joint}^{design}$ , and the decimal part represents the total length  $E_{length}^{design}$ .

The experimental results reveal a diverse set of Pareto solutions. (A) and (B) both have 5 DOFs, but (A) has a

configuration using only rotational joints, while (B) includes a prismatic joint. Both exhibit high performance, with (B) being slightly shorter in total length. (C) has 4 DOFs, insufficient to fulfill all target poses, but it achieves high precision sufficiently. (C) can be considered a configuration with one fewer degree of freedom from (A). (D) and (E) both have 3 DOFs; (D) utilizes only rotational joints, while (E) includes a prismatic joint. Unlike (A) or (C), which only include joints for roll and pitch, (D) includes a yaw joint. (E) is a configuration with 2 fewer DOFs than (B), moving only in a two-dimensional plane with a prismatic joint.

When fitting these configurations into existing robots, (A) and (D), despite having different joint orders, resemble a typical humanoid robot arm with shoulder, elbow, and wrist joints, like in HRP-2 [2]. Such solutions are reasonable for optimization towards Target-ARM, which emulates the workspace of human arms. On the other hand, the structures are not identical; notably, the absence of the yaw joint is a significant difference, driven by the setting that the command values of Target-ARM include almost the same target orientations. (C) has a unique configuration with elbow rotation in the roll direction, different from human arms, but it proved effective in this study's settings. (B) and (E) are examples of effectively using prismatic joints, resembling a replacement of the human elbow with linear actuators. For instance, the surgical robot Da Vinci [19] has a similar configuration. This demonstrates the capability to observe

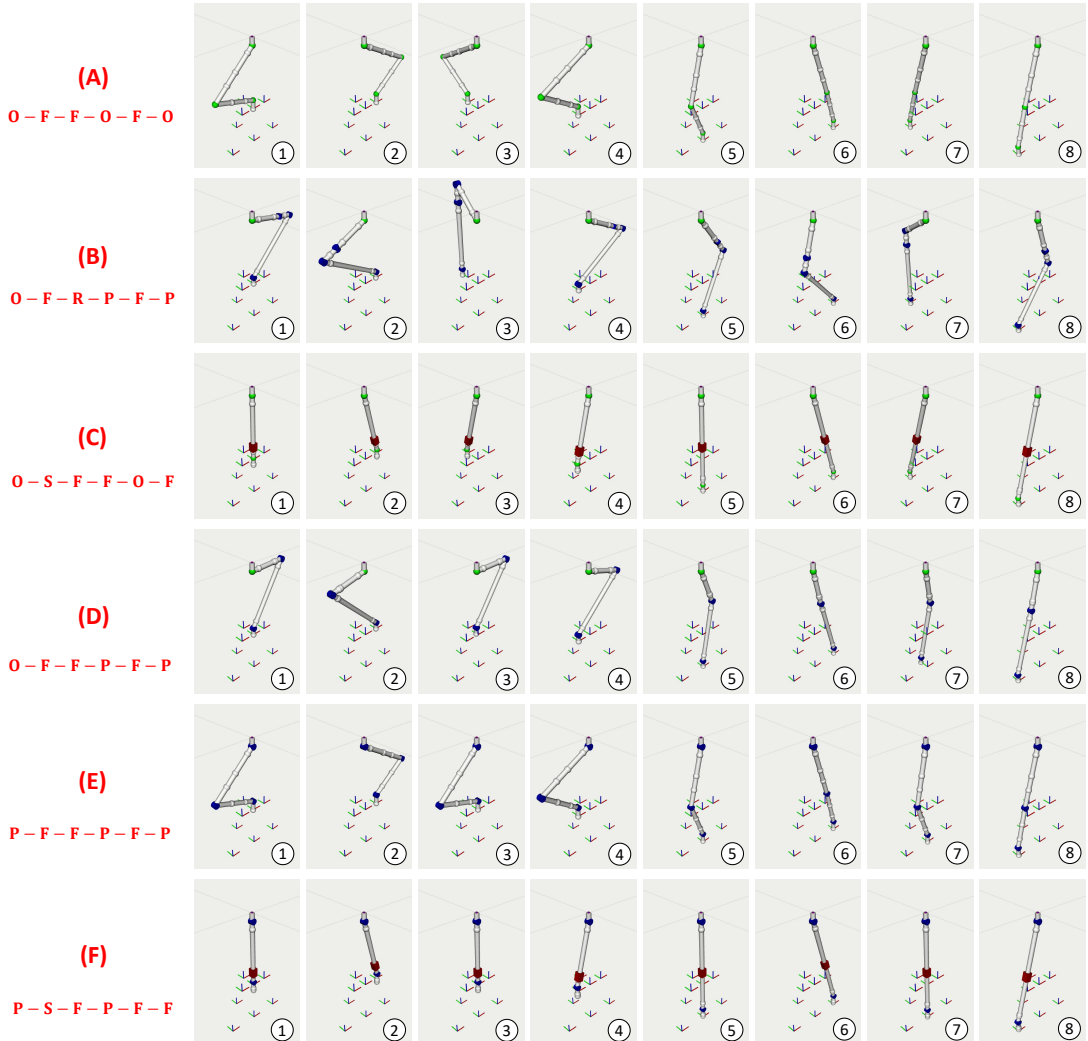


Fig. 8. Several representative Pareto solutions for Target-LEG. Each snapshot shows the result of inverse kinematics for the target position and orientation.

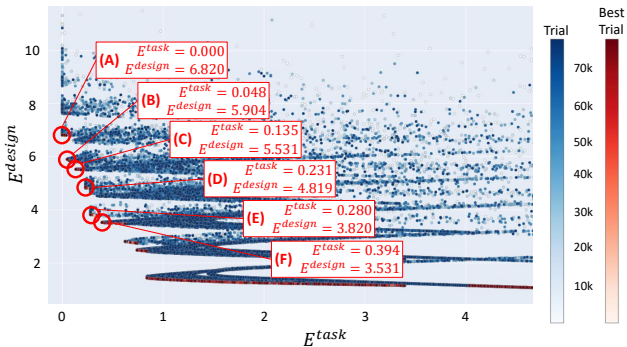


Fig. 9. Sampling results for Target-LEG. Each point represents a solution, with the Pareto solutions highlighted in red. Solutions (A) to (F) are the representative solutions in Fig. 8.

both existing and novel configurations as Pareto solutions simultaneously.

### C. Results for Target-LEG

For Target-LEG, the obtained Pareto solutions are shown in Fig. 8, and the sampling results are shown in Fig. 9. (A) has 6 DOFs, featuring a structure composed of three

consecutive orthogonal two-axis joints, resulting in high task performance. (B) and (C) both have 5 DOFs, with (B) having a configuration similar to (A) but with one fewer degree of freedom, and (C) having a structure with the intermediate orthogonal two-axis joints replaced by a prismatic joint. While the overall length of (A) and (B) is approximately 0.9 m, (C) is significantly shorter with a length of 0.531 m. (D) has 4 DOFs, representing a configuration with one fewer degree of freedom than (B). Finally, (E) and (F) have 3 DOFs each, moving only in a two-dimensional plane. (E) can be considered a configuration with one less degree of freedom than (D), and similarly, (F) can be seen as having one less degree of freedom than (C). The relationships between (A)-(B)-(C) and (D)-(E)-(F) are similar, as evident from the solution arrangement in Fig. 9.

When fitting these configurations into existing robots, (A), (B), (D), and (E) exhibit configurations similar to humanoid robot legs such as HRP-2 [2], featuring legs with hip, knee, and ankle joints. (A) and (E) have thigh and shin links of approximately equal length, while (B) and (D) have much significantly shorter thigh links. Furthermore, since all target

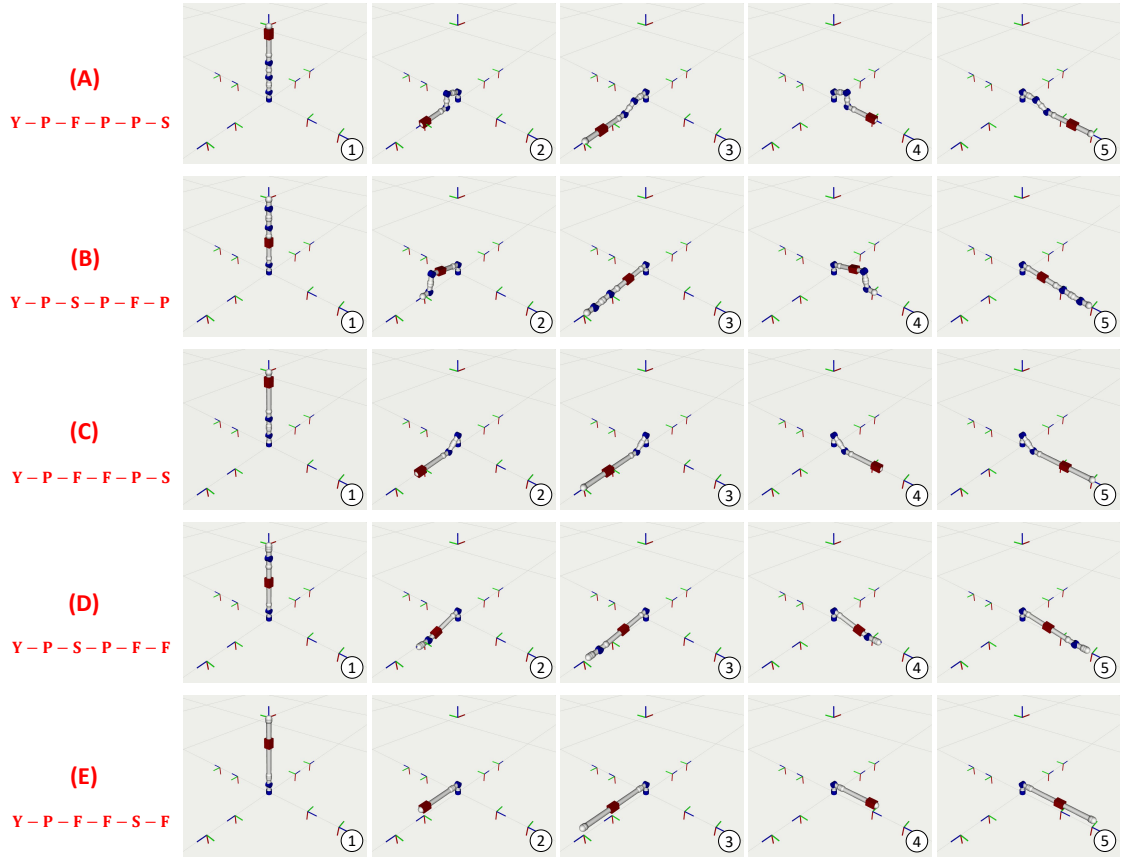


Fig. 10. Several representative Pareto solutions for Target-WIDE. Each snapshot shows the result of inverse kinematics for the target position and orientation.

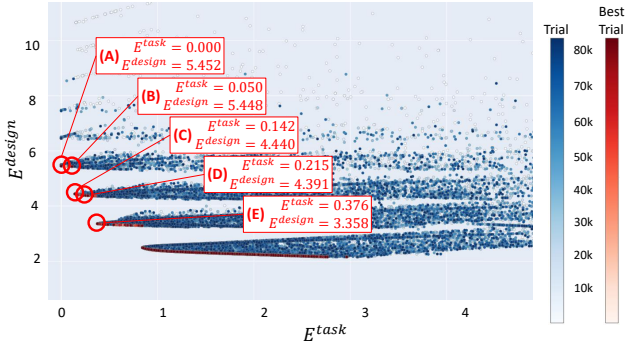


Fig. 11. Sampling results for Target-WIDE. Each point represents a solution, with the Pareto solutions highlighted in red. Solutions (A) to (E) are the representative solutions in Fig. 10.

orientations are aligned, the yaw joint is never used, and the degrees of freedom are constructed solely with roll and pitch. The use of a roll joint in the knee section is a novel and interesting configuration. In conventional legs, the knee typically bends in only one direction, but in the setup of this study, this was not replicated. (C) and (F) showcase examples of effectively utilizing linear joints, resembling a configuration where the human knee section is replaced by a prismatic joint. Similar configurations are observed in robots like SLIDER [4], a humanoid from SCHAFT [3], and a jumping robot RAMIEL [20], albeit with different drive mechanisms. These robots determine the direction of the link

at the root joint, perform vertical movement using a prismatic joint, and control the posture of the foot with ankle joints.

#### D. Results for Target-WIDE

For Target-WIDE, the obtained Pareto solutions are shown in Fig. 10, and the sampling results are shown in Fig. 11. It can be observed that in all cases (A)-(E), prismatic joints are used, and the two joints from the root link are always arranged in the order of yaw and pitch joints. Both (A) and (B) have 5 DOFs each, differing only in the placement of the prismatic joint either at the end or immediately following the yaw and pitch joints. Both (C) and (D) have 4 DOFs each, representing configurations with one less degree of freedom compared to (A) and (B), respectively. (E) has 3 DOFs, constituting the minimal configuration with yaw, pitch, and prismatic joints.

When fitting these configurations into existing robots, (B) and (D) exhibit a body configuration with the same order of yaw, pitch, and prismatic joints as the world's first industrial robot, Unimate. Moreover, (A) and (C) share a similar structure to a shovel excavator, with a prismatic joint at the end to enhance digging performance. Another example with prismatic joints is the Mujin TuckBot [21], where due to its small workspace, the prismatic joint is placed closest to the base, followed by yaw and pitch joints. This contrasts with the configuration seen in setups with a wide workspace like Target-WIDE. Additionally, Fetch [22] employs a prismatic

joint extending in the  $z$  direction from the root link, while a three-axis NC machine has a prismatic joint extending in the  $xy$  direction from the root link. The former is confirmed to occur depending on the setting of the target positions, while the latter cannot meet the constraint of having the links aligned in a straight line in the initial state, so was not observed in the context of this study.

#### IV. CONCLUSION AND FUTURE WORKS

In this study, we explored diverse body configurations in modular robots encompassing both rotational and prismatic joints by utilizing black-box multi-objective optimization. Defining each joint module as a separate Xacro file, we represent various body configurations determined by the arrangement of these joint modules and lengths of the links. By incorporating not only task achievement but also metrics related to the robot's body design into the objective functions, we are able to obtain Pareto solutions of robot configurations with diverse bodies, rather than a single solution. From the experiments, we obtained not only well-established structures commonly found in humanoids and industrial robots but also rare and unconventional body structures. The results from task achievement and body design metrics related to simple kinematics alone yielded highly intriguing findings. This study provides a foundation for exploring new body configurations while considering existing ones in robots with diverse joints.

There are numerous potential extensions for this research. Firstly, further exploration is needed for bodies with a wider variety of joints, including closed-links, wire-driven structures, wheels, and other diverse joint types, in addition to rotational and prismatic joints. Configurations with branching, giving rise to limbs similar to humanoid structures, are also intriguing [14]. To combine more complex structures while maintaining consistency, appropriate constraint conditions must be established, posing a significant challenge for future research. Similarly, there is a need to advance the definition of a more diverse set of objective functions. Evaluating whether existing robot structures are suitable, exploring new structures for various tasks, and experimenting with different objective function designs are crucial aspects. Considering the importance of dynamics, combining control methods such as model predictive control and reinforcement learning is necessary for practical robot structure exploration. Although solutions for several of these challenges already exist, we aim to focus on the autonomous emergence of diverse bodies by combining multiple joint structures in further research.

#### REFERENCES

- [1] "PR2 (Willow Garage)." <http://www.willowgarage.com/pages/pr2/overview>.
- [2] K. Kaneko, F. Kanehiro, S. Kajita, H. Hirukawa, T. Kawasaki, M. Hirata, K. Akachi, and T. Isozumi, "Humanoid robot HRP-2," in *Proceedings of the 2004 IEEE International Conference on Robotics and Automation*, 2004, pp. 1083–1090.
- [3] J. Urata and Y. Ito, "Robotic leg parallel to a ball screw," 2016. [Online]. Available: <https://patents.google.com/patent/US9475191B1/en>
- [4] K. Wang, D. Marsh, R. P. Saputra, D. Chappell, Z. Jiang, A. Raut, B. Kon, and P. Kormushev, "Design and control of SLIDER: an ultra-lightweight, knee-less, low-cost bipedal walking robot," in *Proceedings of the 2020 IEEE/RSJ International Conference on Intelligent Robots and Systems*, 2020, pp. 3488–3495.
- [5] B. Siciliano, "The Tricept robot: Inverse kinematics, manipulability analysis and closed-loop direct kinematics algorithm," *Robotica*, vol. 17, no. 4, pp. 437–445, 1999.
- [6] K. Kawaharazuka, S. Makino, K. Tsuzuki, M. Onitsuka, Y. Nagamatsu, K. Shinjo, T. Makabe, Y. Asano, K. Okada, K. Kawasaki, and M. Inaba, "Component Modularized Design of Musculoskeletal Humanoid Platform Musashi to Investigate Learning Control Systems," in *Proceedings of the 2019 IEEE/RSJ International Conference on Intelligent Robots and Systems*, 2019, pp. 7294–7301.
- [7] S. Yoshimura, S. Yuzaki, K. Kawaharazuka, K. Okada, and M. Inaba, "Optimization of Muscle Arrangement Extraction from Human Waist Structure for Biomimetic Humanoid Implementation," in *Proceedings of the 2023 IEEE-RAS International Conference on Humanoid Robots*, 2023, pp. 583–590.
- [8] G. Yang and I. Chen, "Task-based optimization of modular robot configurations: minimized degree-of-freedom approach," *Mechanism and Machine Theory*, vol. 35, no. 4, pp. 517–540, 2000.
- [9] Y. Xiao, Z. Fan, W. Li, S. Chen, L. Zhao, and H. Xie, "A Manipulator Design Optimization Based on Constrained Multi-objective Evolutionary Algorithms," in *Proceedings of the 2016 International Conference on Industrial Informatics*, 2016, pp. 199–205.
- [10] K. Kawaharazuka, T. Makabe, K. Okada, and M. Inaba, "Daily Assistive Modular Robot Design Based on Multi-Objective Black-Box Optimization," in *Proceedings of the 2023 IEEE/RSJ International Conference on Intelligent Robots and Systems*, 2023, pp. 9970–9977.
- [11] H. S. Kim and L. Tsai, "Design Optimization of a Cartesian Parallel Manipulator," *Journal of Mechanical Design*, vol. 125, no. 1, pp. 43–51, 2003.
- [12] I. B. Hamida, M. A. Laribi, A. Mlika, L. Romdhane, S. Zeghloul, and G. Carbone, "Multi-Objective optimal design of a cable driven parallel robot for rehabilitation tasks," *Mechanism and Machine Theory*, vol. 156, pp. 1–24, 2021.
- [13] K. Kawaharazuka, S. Yoshimura, T. Suzuki, K. Okada, and M. Inaba, "Design Optimization of Wire Arrangement With Variable Relay Points in Numerical Simulation for Tendon-Driven Robots," *IEEE Robotics and Automation Letters*, vol. 9, no. 2, pp. 1388–1395, 2024.
- [14] A. Zhao, J. Xu, M. K. Luković, J. Hughes, A. Spielberg, D. Rus, and W. Matusik, "RoboGrammar: Graph Grammar for Terrain-Optimized Robot Design," *ACM Transactions on Graphics*, vol. 39, no. 6, pp. 1–16, 2020.
- [15] J. Xu, A. Spielberg, A. Zhao, D. Rus, and W. Matusik, "Multi-Objective Graph Heuristic Search for Terrestrial Robot Design," in *Proceedings of the 2021 IEEE International Conference on Robotics and Automation*, 2021, pp. 9863–9869.
- [16] J. Hu, J. Whitman, M. Travers, and H. Choset, "Modular Robot Design Optimization with Generative Adversarial Networks," in *Proceedings of the 2022 IEEE International Conference on Robotics and Automation*, 2022, pp. 4282–4288.
- [17] K. Deb, A. Pratap, S. Agarwal, and T. Meyarivan, "A fast and elitist multiobjective genetic algorithm: NSGA-II," *IEEE Transactions on Evolutionary Computation*, vol. 6, no. 2, pp. 182–197, 2002.
- [18] T. Akiba, S. Sano, T. Yanase, T. Ohta, and M. Koyama, "Optuna: A Next-generation Hyperparameter Optimization Framework," in *Proceedings of the 25th ACM SIGKDD International Conference on Knowledge Discovery and Data Mining*, 2019.
- [19] C. Freschi, V. Ferrari, F. Melfi, M. Ferrari, F. Mosca, and A. Cuschieri, "Technical review of the da Vinci surgical telemanipulator," *The International Journal of Medical Robotics and Computer Assisted Surgery*, vol. 9, no. 4, pp. 396–406, 2013.
- [20] T. Suzuki, Y. Toshimitsu, Y. Nagamatsu, K. Kawaharazuka, A. Miki, Y. Ribayashi, M. Bando, K. Kojima, Y. Kakiuchi, K. Okada, and M. Inaba, "RAMIEL: A Parallel-Wire Driven Monopodal Robot for High and Continuous Jumping," in *Proceedings of the 2022 IEEE/RSJ International Conference on Intelligent Robots and Systems*, 2022, pp. 5017–5024.
- [21] "TuckBot (Mujin)." <https://mujin-corp.com/truckbot-automated-truck-unloader/>.
- [22] "Fetch (Fetch Robotics)." <https://fetchrobotics.com/>.